
Since January 2020 Elsevier has created a COVID-19 resource centre with free information in English and Mandarin on the novel coronavirus COVID-19. The COVID-19 resource centre is hosted on Elsevier Connect, the company's public news and information website.

Biosensors and Bioelectronics 215 (2022) 114570

Contents lists available at ScienceDirect

Biosensors and Bioelectronics

journal homepage: www.elsevier.com/locate/bios

# Directly immersible silicon photonic probes: Application to rapid SARS-CoV-2 serological testing

Michailia Angelopoulou [a], Eleni Makarona [b], Alexandros Salapatas [b], Konstantinos Misiakos [b], Evgenia Synolaki [c], Anastasios Ioannidis [d], Stylianos Chatzipanagiotou [e], Mikael A. Ritvos [f,g,h], Arja Pasternack [f], Olli Ritvos [f], Panagiota S. Petrou [a,*], Sotirios E. Kakabakos [a]

[a] Institute of Nuclear & Radiological Science & Technology, Energy & Safety, NCSR "Demokritos", Aghia Paraskevi, 15341, Greece
[b] Institute of Nanoscience and Nanotechnology, NCSR "Demokritos", Aghia Paraskevi, 15341, Greece
[c] Centre for Clinical, Experimental Surgery and Translational Research, Biomedical Research Foundation Academy of Athens, Athens, 11527, Greece
[d] Department of Nursing, Faculty of Health Sciences, University of Peloponnese, Tripoli, 22100, Greece
[e] Department of Medical Biopathology and Clinical Microbiology, Aeginition Hospital, Medical School, National and Kapodistrian University of Athens, Athens, 11528, Greece
[f] Department of Physiology, Faculty of Medicine, University of Helsinki, Helsinki, 00014, Finland
[g] School of Engineering Sciences in Chemistry, Biotechnology and Health, KTH Royal Institute of Technology, Stockholm, Sweden
[h] Nordic SARS Response AB, Stockholm, 19455, Sweden

ARTICLE INFO

*Keywords:*
Immersible sensor
Silicon nitride waveguides
Broad-band Mach-Zehnder interferometry
Label-free detection
SARS-CoV-2 antibody

ABSTRACT

Silicon photonic probes based on broad-band Mach-Zehnder interferometry are explored for the first time as directly immersible immunosensors alleviating the need for microfluidics and pumps. Each probe includes two U-shaped waveguides allowing light in- and out-coupling from the same chip side through a bifurcated fiber and a mechanical coupler. At the opposite chip side, two Mach-Zehnder interferometers (MZI) are located enabling real-time monitoring of binding reactions by immersion of this chip side into a sample. The sensing arm windows of the two MZIs have different length resulting in two distinct peaks in the Fourier domain, the phase shift of which can be monitored independently through Fast Fourier Transform of the output spectrum. The photonic probes analytical potential was demonstrated through detection of antibodies against SARS-CoV-2 in human serum samples. For this, one MZI was functionalized with the Receptor Binding Domain (RBD) of SARS-CoV-2 Spike 1 protein, and the other with bovine serum albumin to serve as reference. The biofunctionalized probes were immersed for 10 min in human serum sample and then for 5 min in goat anti-human IgG Fc specific antibody solution. Using a humanized rat antibody against SARS-CoV-2 RBD, a detection limit of 20 ng/mL was determined. Analysis of human serum samples indicated that the proposed sensor discriminated completely non-infected/non-vaccinated from vaccinated individuals, and the antibodies levels determined correlated well with those determined in the same samples by ELISA. These results demonstrated the potential of the proposed sensor to serve as an efficient tool for expeditious point-of-care testing.

## 1. Introduction

During the past two decades, the progress in micro/nano-fabrication techniques and in-depth understanding of photonic circuits has allowed the development of optical biosensing modules based on silicon substrates. These sensing modules take advantage of the fact that silicon-based photonic integrated circuits can be manufactured at high volume and relatively-low cost while there is possibility to fabricate multiple sensors on a single chip (Luan et al., 2018; Shakoor et al., 2019). In addition, the high refractive index contrast between silicon and silicon dioxide/silicon nitride or other surrounding media, facilitates light coupling and light guiding in curved waveguides thus enabling the label-free sensing of affinity interactions between an analyte and a receptor molecule in real-time with high detection sensitivity (Luan et al., 2018; Shakoor et al., 2019). Nonetheless, despite the impressive progress, very few of the existing silicon photonic integrated circuits have managed to escape laboratory settings and evolve to commercially available instruments which, however, are benchtop instruments not

* Corresponding author. Research Immunoassays/Immunosensors Lab. INRASTES NCSR "Demokritos", 15341 Aghia Paraskevi, Greece.
*E-mail address:* ypetrou@rrp.demokritos.gr (P.S. Petrou).

https://doi.org/10.1016/j.bios.2022.114570
Received 20 April 2022; Received in revised form 7 July 2022; Accepted 9 July 2022
Available online 12 July 2022

suitable for point-of-need applications. The main reason is that silicon inherently does not emit light and there is always the need to find a way to couple light in and out of the photonic chips. Thus, even though the chips themselves are miniaturized and compact, their driving and readout system requirements render their use in everyday life more or less impractical.

The emergence of the COVID-19 pandemic revealed once more the need for point-of-care systems with high clinical sensitivity and specificity and minimal intervention from the user for detection of the virus or antibodies against it in biological samples (Mattioli et al., 2020). The latter application is very important in seroprevalence studies, which examine the SARS-CoV-2 infection spread in a community (Amanat et al., 2020; Eckerle and Meyer, 2020; Fotis et al., 2021; Jalkanen et al., 2021a), as well as the vaccination efficiency (Jalkanen et al., 2021b) and our understanding of the immunity progress over time (Okba et al., 2020). In this context, several approaches of serological testing based on lateral flow immunoassay (LFIA) or biosensors have been exploited for the point-of-care detection of total antibodies against SARS-CoV-2 in human serum. LFIAs are suitable for fast point-of-care as well as self-diagnostic tests due to their ease of use and short analysis time (Feng et al., 2020; Liu et al., 2020, 2021; Roda et al., 2021; Wang et al., 2020; Wen et al., 2020). However, in most cases, they provide mainly qualitative results with sensitivity and specificity lower than those obtained by laboratory-based immunochemical methods (Lisboa Bastos et al., 2020). Biosensors on the other hand, could provide high detection sensitivity complimented by short turn-around times and ease-of-use (Antiochia, 2021). So far, several biosensing principles have been exploited for the detection of antibodies against SARS-CoV-2 in human serum, most of which are relying on optical (Cady et al., 2021; Dzimianski et al., 2020; Funari et al., 2020; Shaw et al., 2020; Steiner et al., 2020) or electrochemical transducers (Ali et al., 2020; Rashed et al., 2021; Torrente-Rodrıguez et al., 2020; Yakoh et al., 2021). Regarding the SARS-CoV-2 protein used for detection of serum antibodies, most sensors rely on spike glycoprotein S1 and/or S2 subunit or fragments thereof, such as the spike receptor binding domain (RBD) (Ali et al., 2020; Dzimianski et al., 2020; Funari et al., 2020; Rashed et al., 2021; Shaw et al., 2020; Steiner et al., 2020; Yakoh et al., 2021). Although all these sensors provided rapid analysis with good analytical and clinical sensitivity, most of them involve fluidic modules and external pumping systems or bulk instrumentation (especially the optical ones) that complicate or restrict their application at the point-of-care.

In order to fulfil the stringent requirements of point-of-need testing, arrays of fully integrated Broad-band Mach-Zehnder Interferometers (Misiakos et al., 2014a, 2014b; Makarona et al., 2016) have been developed and implemented in our previous works in a variety of applications ranging from the detection of harmful substances in different food matrices (Angelopoulou et al., 2015; Pagkali et al., 2017, 2018; Angelopoulou et al., 2018) to the detection of disease markers in human serum (Psarouli et al., 2017). In particular, the chips employed in these works included ten Broad-band Mach-Zehnder Interferometers (BB-MZIs) along with their respective silicon light emitting diodes allowing multiplexed determination by spatially selective biofunctionalization of BB-MZIs of a single chip (Pagkali et al., 2018; Angelopoulou et al., 2018). By integrating onto the chip the spectrum analyser (Misiakos et al., 2019), the ultimate degree of integration of all passive and active components on a single chip was achieved leading to a really portable instrument. Despite the small chip and instrumentation size, the complexity of fluidic and electronic connections as well as the high cost of chip fabrication limited its wide application.

In this work, an alternative chip design, based on integrated photonic circuits (PICs), is introduced requiring a much simplified fabrication process suitable for mass production at minimum costs while keeping the advantages of broad-band MZI. The new approach integrates only the passive optical components in an elongated rectangle chip which interacts with the environment through its short sides. The chip features two U-shaped waveguides structured as MZIs and laid out so as their input and output waveguides are located on one of the short chip sides and adjacent to the two branches of the bifurcated fiber that provides the optical interconnects to the spectrometer and a broad-band light source (Fig. 1a). On the opposite free end of the chip lay the sensing arms of the two integrated MZIs to be immersed in the sample (US Patent 11,119,040; EPO Patent Application: EP3532825A1). In a sense the integrated interferometers connect the light source to the spectrometer while they modulate the broad spectrum and produce interference fringes. A specially-designed optomechanical adapter aligns the chip input-output waveguides to the bifurcated fiber branches. No extra optical components such as lenses or polarizers are required. The elongated format of the chips provides for the physical separation between the light port and the sensing area, and enables its direct immersion in the sample to be analyzed as a dip-stick probe, thus rendering the use of microfluidics nonessential (Fig. 1b). In addition, the chip design enables one MZI to be used, after appropriate functionalization, for the monitoring of the specific immunoreaction (working sensor), and the other to be used as reference to compensate for the non-specific binding signal and matrix effect (reference sensor). Demultiplexing of the two interferometers signal is done through Fourier Transform in the wavenumber domain as the two interferometers have distinct frequencies in their interference fringes due to different sensing arm lengths (Misiakos et al., 2014a). The final measuring system is assembled with a low-cost white light emitting diode (LED) as the input source and a commercial miniaturized spectrophotometer as the recording medium, leading to a lightweight system that is controlled through a custom-designed software installed in a laptop and powered through a USB connection from the same laptop (Figs. S1a and S1b). For the detection of antibodies against SARS-CoV-2, the sensing window of working MZI was spotted with a solution of SARS-CoV-2 RBD domain peptide (working sensor), while the window of the reference MZI with blocking protein (reference sensor). Several parameters of the photonic probe biofunctionalization were studied and optimized including the chemical activation of the surface and the immobilization of the RBD peptide, as well as parameters related to the assay, i.e., the composition of serum diluent and the dilution implemented, the duration of biofunctionalized probe immersion into the sample, and the implementation of a secondary goat anti-human IgG Fc specific antibody in order to follow changes of IgG concentration and improve the detection sensitivity. The evaluation of the serological test developed was performed using human serum samples from non-infected/non-vaccinated individuals and vaccinated ones.

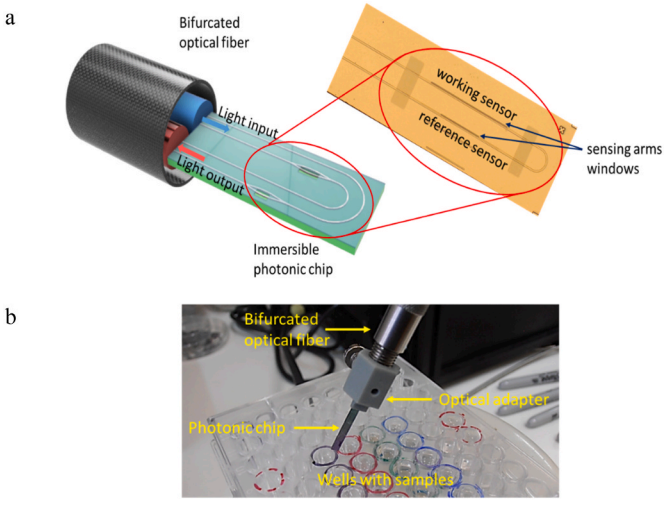


**Fig. 1.** (a) Schematic representation of the photonic integrated circuit (PIC) probe (not in scale) and a close-up microscope image of the immersible probe side. The working and reference MZIs sensing arm windows length is 2 and 1 mm, respectively. (b) Image of the PIC probe just before it is immersed in a sample. The optical adapter and the bifurcated optical fiber are also shown.

The results obtained with the sensor were compared to those provided for the same samples by an in-house developed ELISA for the determination of anti-SARS-CoV-2 IgG titer in human sera. The findings demonstrate the potential of the proposed system to become a powerful tool for expeditious quantitative serological testing for antibodies against SARS-CoV-2.

## 2. Materials and methods

### 2.1. Reagents

The recombinant receptor binding domain (RBD) covering amino acids 319–547 of the SARS-CoV-2 virus spike protein and flanked with a C-terminal 8xHis tag was expressed in stably transfected HEK293F cells and purified by Ni-agarose immobilized metal chelate affinity chromatography as previously described (Jalkanen et al., 2021a). A recombinant full-sized chimeric monoclonal antibody with wild type variable domains of rat monoclonal antibody and human IgG1 constant domains against the SARS-CoV-2 S1 subunit protein RBD domain (code RBD5305) was obtained from HyTest Ltd. (Turku, Finland). Bovine serum albumin (BSA), mouse γ-globulins, glutaraldehyde (25% w/v aqueous solution), (3-aminopropyl)triethoxysilane (APTES), and 2, 2′-azino-bis (3-ethyl-benzothiazoline-6-sulfonic acid) diammonium salt (ABTS) were purchased from Sigma-Aldrich Chemie GmbH (Taufkirchen, Germany). Alexa Fluor 488 labeled goat anti-mouse IgG antibody, and anti-human IgG Fc specific antibody produced in goat were from Thermo Fisher Scientific (Waltham, MA, USA). Goat anti-human IgG (whole molecule) antibody conjugated to horse radish peroxidase (HRP) was obtained from Bio-Rad Laboratories Inc. Tris(hydroxymethyl)aminomethane (Tris) and all the other reagents used were from Merck (Darmstadt, Germany). Microtiter plates were purchased from Greiner Diagnostic GmbH (Bahlingen, Germany). Anonymized human serum samples, 25 from vaccinated and 12 from non-infected/non-vaccinated individuals, were provided from the Department of Clinical Microbiology of Aeginition Hospital, Medical School, National and Kapodistrian University of Athens, Greece, after approval of the procedure by the hospital's ethics committee (Reference number 27/27-01-2022).

### 2.2. Silicon photonic probe fabrication and principle of operation

The silicon chips with the photonic integrated circuits (PIC) have been fabricated at the clean-room facility of the Nanotechnology and Microsystems Laboratory, Institute of Nanoscience and Nanotechnology, NCSR "Demokritos", on 4″-wafers with a 3 μm-thick silicon dioxide bottom cladding layer (SiMat, Kaufering, Germany). The process consists of standard microfabrication techniques and includes LPCVD deposition of a silicon nitride layer, two optical lithography steps and a dry etching step for the definition of the photonic circuit waveguides, deposition of a 2 μm-thick silicon dioxide top cladding layer, photolithography and a wet etching step for the definition of the MZIs sensing windows over one of their arms while the other stays covered by the top cladding layer. After completion of the process, the wafers were diced to 25 mm × 2.0 mm individual chips. The two MZIs of a single chip have different sensing arm windows lengths; the working has a 2 mm x 20 μm window while the reference one has a 1 mm x 20 μm window. The waveguide engineering of the photonic integrated circuit (PIC) of the chips secures efficient light coupling, low optical propagation losses, and external polarizer-free selection of the $TM_{00}$-mode necessary for the operation of the MZIs along a 300 nm-wide band in the VIS-NIR (600–900 nm). These features are achieved by appropriate combinations of rib and ridge waveguides of varying geometrical features and lateral tapers for mode filtering based on rigorous simulations, which ensured the optimal performance of each PIC component.

### 2.3. Instrumentation

The bioanalytical platform consists of a custom-made reader, the biofunctionalized photonic probes, and a laptop that runs the dedicated software and powers up the system (schematically depicted in Fig. S1a and shown in Fig. S1b). The reader consists of a broad-band high brightness white LED (Ushio Europe B.V.; Oude Meer, Netherlands) and VIS-NIR spectrophotometer (Flame-T-VIS-NIR, Ocean Insight), both coupled to the photonic probes via a 400 μm-core bi-furcated optical fiber (Ocean Insight; Duiven, The Netherlands) and a specially-designed optical adapter fabricated by 3D printing (Fig. 1b). The two adjacent MZIs (sensing and reference) have a lateral separation of 30 μm, whereas the distance of the light input and output ports is about 480 μm to match the core-to-core separation of the 400 μm-core bifurcated fiber plus the thickness of cladding layers around the fiber core. In fact, the sensing MZI has an input-output separation slightly larger than the reference MZI one due to their 30-μm distance. To achieve high coupling efficiency, ideally single mode fibers could have been used butt-coupled to integrated single mode waveguides of similar dimensions. In our case, however, due to mechanical constraints and to compensate for alignment tolerances, the fiber cores are much larger (400 μm) than the waveguide dimensions leading to multimode fibers. This disparity in the input fiber-input waveguide cross sections results in low in-coupling light efficiency. On the other hand, the coupling efficiency from the output waveguide to the output fiber is high as the waveguide emits the light near the core center and at small angles. The LED is mounted on an in-house developed heat sink and driving PCB board. In Fig. S2, the emission spectrum of the LED as recorded by the spectrophotometer used is provided. Both the LED and the spectrophotometer are powered through a USB by the same laptop that runs the dedicated software for signal acquisition and real-time analysis of the results. The software comprises two major components: (i) the signal recording and processing algorithm, and (ii) the user interface that allows the user to observe the signal evolution in real time (Fig. S1c). Since the two BB-MZIs contained in the photonic probes are engineered to have their own distinct peaks in the Fourier domain, the two peaks can be independently tracked by monitoring their phases. Hence, the signal processing algorithm collects the spectra recorded by the spectrophotometer, performs in real-time discrete Fast Fourier Transform (FFT) of each recorded spectrum, and continuously monitors the two peak phases expressed in radians as they evolve in time (in manner analogous to the method analyzed by Misiakos et al., 2014a).

### 2.4. Photonic probe chemical activation and biofunctionalization

Selective chemical activation of the silicon nitride area exposed at the sensing windows versus the surrounding silicon dioxide was performed following a literature protocol (Banuls et al., 2010). In brief, the chips were cleaned by sequential 10-min sonication in baths of acetone and isopropanol prior to immersion in 1% (v/v) hydrofluoric acid (HF) solution in deionized water for 3 min at room temperature (RT). After thorough washing with deionized water and drying with nitrogen stream, the chips were immersed in a 2.5% (w/v) glutaraldehyde solution in 0.01 M phosphate buffer saline (PBS), pH 7.4, and incubated for 2 h at RT. The chips were washed with PBS and deionized water and dried with nitrogen stream prior to spotting of biomolecules. Spotting was performed using a BioOdyssey Calligrapher Mini Arrayer (Bio-Rad Laboratories Inc.; Hercules, CA) equipped with a quill pin with 62.5 μm tip diameter (Arrayit Corp., Sunnyvale, CA). Multiple overlapping spots of a 1 mg/mL RBD SARS-CoV-2 peptide or BSA solution in 0.01 M PBS, pH 7.4, were deposited along the sensing windows of the working and the reference sensor of each chip, respectively. The chips were left at RT for 1 h and 65% humidity to allow for binding of the proteins to the sensing windows areas, prior to washing with PBS and blocking through immersion for 1 h in PBS containing 10 mg/mL BSA. After that, the chips were washed with PBS and deionized water dried under a nitrogen

stream and used for the assay.

### 2.5. Assay for detection of total antibodies against COVID19 with the bioanalytical platform

Human serum samples diluted 50 times with assay buffer (0.05 M Tris-HCl, pH 7.6, 9 g/L NaCl, 5 g/L BSA) were added in the wells of a microtitration plate (300 μL per well). The biofunctionalized chip was immersed for 2 min in assay buffer, 10 min in the diluted serum sample, 2 min in assay buffer, and then for 5 min in a 10 μg/mL of goat anti-human IgG Fc specific antibody solution in assay buffer. Finally, the chip was immersed in assay buffer for a few min. The chip signal (S) corresponding to each run is calculated according to the equation:

$$S = \Delta\varphi_{Work} - \left(2 * \Delta\varphi_{Ref}\right)$$

where $\Delta\varphi_{Work}$ is the phase shift due to reaction in the working sensor, and $\Delta\varphi_{Ref}$ is the phase shift determined for the reference sensor multiplied by 2 to account for the length difference of the sensor windows. To calculate the phase shift difference of each sensor, the mean value of 300 data points acquired while the chip is immersed in assay buffer prior to and after the reaction were taken into account to compensate for the fluctuation of sensors response.

## 3. Results and discussion

### 3.1. Chemical and biochemical functionalization of PIC chips

For the detection of the anti-SARS-CoV-2 antibodies in human serum samples, the window area of the working sensor was modified with the RBD SARS-CoV-2 peptide and that of the reference one with blocking protein, e.g., BSA, to provide the non-specific binding signal for each sample. The binding of these proteins preferably on the silicon nitride area defined by the window required appropriate chemical functionalization of the chip surface. Thus, a protocol based on chip treatment with HF in order to create secondary amine groups selectively onto silicon nitride was applied (Banuls et al., 2010). These secondary amine groups were then reacted with glutaraldehyde to introduce reactive aldehyde groups onto the surface which were then employed for covalent binding of RBD peptide via reaction with the primary amine groups in the RBD molecule, mainly ε-amine groups of lysine residues. In addition, a non-selective surface modification with APTES was also applied (the detailed protocol is provided in Supplementary material), to enable immobilization of the RBD peptide onto the chip surface through physical adsorption (Angelopoulou et al., 2015, 2018; Gajos et al., 2016; Psarouli et al., 2017; Pagkali et al., 2017, 2018; Misiakos et al., 2019). The two protocols were tested employing mouse IgG as biomolecule to be immobilized onto the chips and a fluorescently labeled anti-mouse IgG antibody for detection of surface bound biomolecules. As it can be concluded from the fluorescence microscope images provided in Fig. S3, the treatment with HF/glutaraldehyde resulted in selective functionalization of silicon nitride versus the surrounding silicon dioxide surface (Fig. S3a), while modification with APTES did not provide selective functionalization of silicon nitride versus silicon dioxide, but in the contrary promoted binding of the protein molecules to the silicon dioxide than to silicon nitride area (Fig. S3b). The two surface activation methods were also evaluated using chips spotted with the RBD peptide and probed with a humanized rat monoclonal anti-RBD antibody. Characteristic real-time responses of both the working and reference sensor of PIC chips functionalized either by HF/glutaraldehyde or APTES were provided in Figs. S3c and S3d, respectively. The mean response (±1 standard deviation) obtained by 3 chips modified with APTES after a 10-min immersion in the antibody solution (10 μg/mL) was 3.18 (±0.21) rad whereas the mean response from 3 chips functionalized applying the HF/glutaraldehyde method was 3.42 (±0.19) rad. Regarding the response of the reference sensor, in case of HF/glutaraldehyde method, it was within the mean value ± 3 standard deviations (SD) of baseline variation, whereas in case of functionalization with APTES, despite low, it was clearly distinguished from the baseline signal. Thus, the HF/glutaraldehyde surface chemical functionalization protocol was selected for further experimentation.

After the selection of chips chemical functionalization, the binding of the SARS-CoV-2 RBD domain peptide and BSA onto the respective windows of the working and reference sensors of the PIC chips was optimized. For the spatial deposition of the protein solutions onto the respective sensor window, a contact printing spotter was employed. Two different types of pins have been compared, a solid pin with a tip diameter of 375 μm that deposited approximately 12 nL of solution per spot and a quill pin with 62.5 μm tip diameter and delivery volume of approximately 0.5 nL per spot. Either pin required the application of multiple overlapping spots in order to cover the whole length of the windows on both the working and the reference sensing arm. Thus, in order to cover completely the sensing arm window with the solid pin 20 spots were deposited corresponding to 240 nL, whereas with the quill pin 46 spots were deposited corresponding to 23 nL. Despite, the considerable difference in the liquid volume deposited, there was no statistically significant difference in the response of the chips spotted with the solid rather than the quill pin. In particular, the mean response from 3 chips (±1 standard deviation) spotted with the quill pin and assayed by immersion in a 10 μg/mL humanized rat monoclonal anti-RBD antibody solution for 10 min was 3.38 (±0.21) rad, whereas the respective mean value of 3 chips spotted with the solid pin was 3.35 (±0.24) rad. On the other hand, the time required to spot both windows of a single chip was reduced from approximately 7 min required with the solid pin to less than 1 min using the quill. Therefore, it was opted that both the deposition of the RBD-domain peptide solution onto the windows of the working sensor and the BSA solution onto that of the reference sensor was performed with the quill pin.

The RBD peptide concentration used for coating of the chips working sensor was also determined using concentrations ranging from 100 to 1200 μg/mL. As shown in Fig. 2a, the chip response increased as the concentration of the RBD peptide in the coating solution increased and reached a plateau for concentrations equal to or higher than 1000 μg/mL. Therefore, this concentration was used for coating of the chips. A bovine serum albumin (BSA) solution of the same concentration was used to spot the sensing arm windows of the reference BB-MZIs.

### 3.2. Assay optimization

The assay to determine the anti-SARS-CoV-2 antibodies in human serum is performed by immersion of the biofunctionalized chips into diluted human serum. Thus, two critical parameters had to be determined, the serum diluent composition and the dilution factor. To determine the most appropriate serum diluent, or assay buffer as it would be mentioned hereinafter, the following buffers were tested: 0.05 M phosphate buffered saline (PBS), pH 7.4, 0.05 M phosphate buffered saline (PBS), pH 7.4, 0.5 M KCl, 0.05 M Tris-HCl buffer, pH 7.6, 9 mg/mL NaCl, and 0.05 M Tris-HCl buffer, pH 7.6, 9 mg/mL NaCl, 0.5 M KCl. All buffers contained 5.0 mg/mL BSA. The chip signals obtained after immersion for 10 min in a 10 μg/mL solution of humanized rat monoclonal anti-RBD antibody are provided in Fig. 2b. As can be seen, 0.05 M Tris-HCl buffer, pH 7.6, provided higher signals than the 0.05 M PBS buffer, pH 7.4. The inclusion of KCl in the assay buffer was examined, since it could suppress the serum effect with the assumption that its presence would not affect the chip signal. However, as indicated by the data presented in Fig. 2b, the presence of KCl in assay buffer resulted in significant reduction of the chip signal and, therefore, it was not included in the assay buffer finally selected (0.05 M Tris-HCl buffer, pH 7.6, containing 5.0 mg/mL BSA and 9 mg/mL NaCl).

After the selection of the assay buffer, the serum dilution that provided the highest specific and the lowest non-specific signal was determined. For this purpose, chips equilibrated with assay buffer were

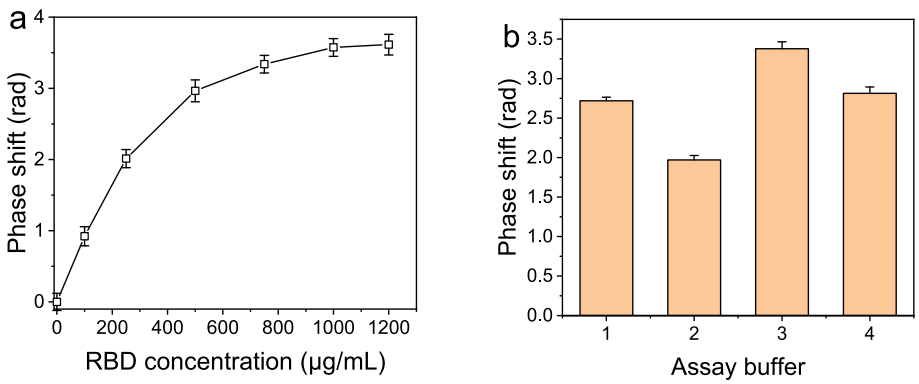


**Fig. 2.** (a) Responses obtained using chips functionalized by HF/glutaraldehyde and coated with RBD peptide solutions with concentration ranging from 100 to 1200 μg/mL upon immersion for 10 min in a 10 μg/mL humanized rat monoclonal anti-RBD antibody solution. Each point is the mean value of three measurements ± SD. (b) Chip responses obtained upon immersion for 10 min in a 10 μg/mL humanized rat monoclonal anti-RBD antibody solution prepared in (1) 0.05 M PBS, pH 7.4, (2) 0.05 M PBS, pH 7.4, 0.5 M KCl, (3) 0.05 M Tris-HCl buffer, pH 7.6, 9 mg/mL NaCl, and (4) 0.05 M Tris-HCl buffer, pH 7.6, 9 mg/mL NaCl, 0.5 M KCl. All buffers contained 5.0 mg/mL BSA. Each point is the mean value of three measurements ± SD.

immersed in a 10 μg/mL humanized rat monoclonal anti-RBD antibody solution (one step assay) prepared either in assay buffer or SARS-CoV-2 negative serum sample diluted with assay buffer 10, 20, 50 or 100 times. After the reaction, the chips were immersed in assay buffer to wash out the serum. The phase shift difference of both the working (green bars) and reference sensor (orange bars) when immersed in assay buffer after and prior to reaction are presented in Fig. S4a. In addition, the chip net signals are also included (purple bars). As shown, by decreasing the serum dilution from 100 to 10 times, a considerable increase of the reference sensor signal was observed especially for dilution equal to or lower than 20 times, which resulted in a 20–25% net signal decrease (purple bars in Fig. S4a). This could be ascribed to the fact that the high protein content of the serum interferes with the specific binding reaction between the immobilized antigen and the anti-RBD antibody in the sample. On the other hand, when the serum dilution was 50 or 100 times, the chip net signal values were not affected compared to the signal obtained when the reaction took place in assay buffer.

Furthermore, in order to increase the signal and to detect specifically the anti-SARS-CoV-2 IgG in the sample, immersion in a solution of an antibody against the Fc fragment of human IgGs for 5 min was introduced followed by immersion in assay buffer. The signals obtained after reaction with this secondary antibody (two steps assay) for different serum dilutions are presented in Fig. S4b. As shown, an approximately three-fold signal increase was observed for all serum dilutions tested. However, the signals obtained using serum diluted 10 or 20 times were lower than those received using higher serum dilutions or assay buffer, supporting the assumption that the specific immunoreaction of the immobilized SARS-CoV-2 RBD with the antibody was hindered by the high serum protein content and the associated non-specific binding. Thus, in order to eliminate the serum effect, a 50-times serum dilution was selected for further experimentation. In Fig. 3, the real-time responses of the working (red line) and the reference (black line) sensor of a chip along with the chip net signal (blue line) upon reaction for 10-min with a 50-times diluted serum sample obtained from a vaccinated individual followed by a 5-min reaction with anti-human IgG Fc specific antibody are presented. As shown, the introduction and washing out of the diluted serum caused abrupt signal changes to both sensors which were, however, almost eliminated when the chip net signal was considered. The chip net signal increase achieved after reaction with the secondary antibody is also expected to improve the assay analytical sensitivity.

### 3.3. Analytical sensitivity of the assay

The analytical sensitivity of the sensor developed was determined using a humanized rat monoclonal anti-RBD antibody at concentrations ranging from 0.05 to 20 μg/mL in 50-times diluted negative serum. The chip net signal values received after a 10-min immersion in the antibody solution (one step assay) are depicted in Fig. 4a, along with the respective values when an additional reaction step with an anti-human

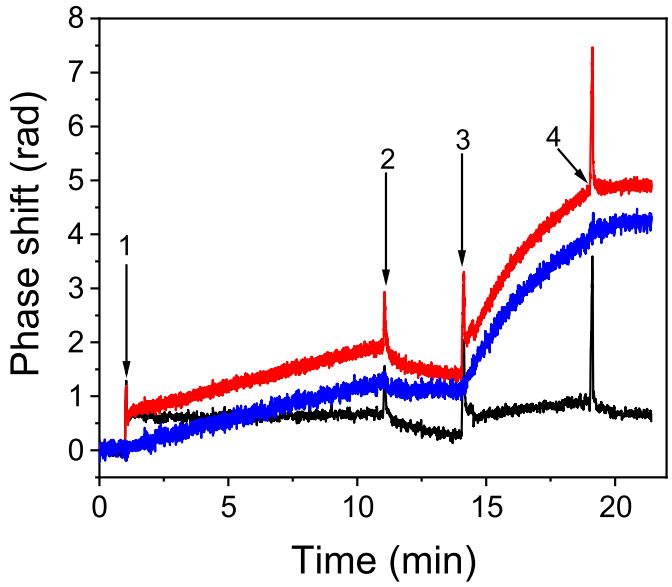


**Fig. 3.** Real-time responses obtained from the working (red line) and the reference sensors (black line) of a chip immersed in a serum sample from a vaccinated individual diluted 50-times with assay buffer for 10 min (arrow 1 to 2), followed by immersion to assay buffer for 3 min (arrow 2 to 3), a 10 μg/mL goat anti-human IgG Fc specific antibody solution for 5 min (arrow 3 to 4), and finally to assay buffer (arrow 4 to end). Blue line corresponds to the chip net signal. The "spikes" in the signals correspond to the transfer of the immersible chips from well to well.

IgG Fc specific antibody (two steps assay) was employed. The detection limit was defined as the antibody concentration corresponding to +5SD of 10 measurements of zero concentration of humanized rat monoclonal antibody, performed with 10 different chips, and was found to be 80 and 20 ng/mL for the direct binding assay and the assay involving the additional reaction with the anti-human IgG Fc specific antibody, respectively. This 4-fold improvement in detection sensitivity when the reaction with the anti-human IgG Fc specific antibody was included in the assay protocol might be crucial when samples with low content in antibodies against SARS-CoV-2 are analyzed.

The intra-assay repeatability of the sensor response was tested by running 1 negative and 2 positive samples in triplicate within a day and the percent coefficient of variation (CV) ranged from 3.6 to 5.7%, while the inter-assay repeatability was evaluated by running the same samples in duplicate in six different days within a period of two months and the CV ranged between 6.9 and 8.6%. The sensor-to-sensor repeatability was also evaluated by running the same sample in five sensors in the same day and the CV was found to be 5.4%. The stability of the sensor was also tested using sensors that were either kept for a month in the

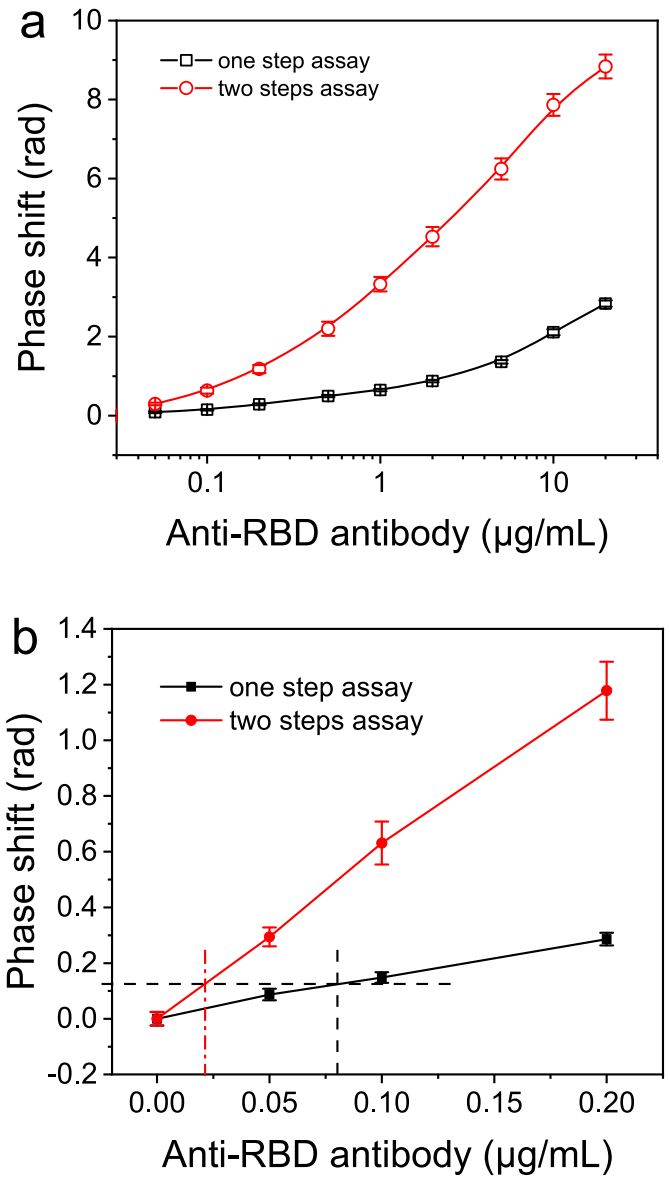


**Fig. 4.** (a) Dose response curves received after a 10-min reaction with solutions of a humanized rat monoclonal anti-RBD antibody in 50-time diluted negative serum (black line) or an assay involving an additional 5-min reaction step with anti-human IgG Fc specific antibody (red line). Each point is the mean value of three measurements ± SD (ten measurements for zero antibody concentration). (b) A magnified view of (a) to determine the detection limit of the assay involving direct binding of the anti-RBD antibody (black line) and the assay involving an additional 5-min reaction step with anti-human IgG Fc specific antibody (red line). The dashed horizontal line corresponds to signal equal to +5SD of the mean signal obtained for the zero antibody concentration, while the vertical dashed lines indicate the detection limits of the two assays.

refrigerator immersed in buffer or after washing with distilled water and drying. It was found that the sensor response was stable under both storage conditions, with the difference that the dried sensors required an initial immersion in assay buffer for at least 5 min to receive a stable baseline signal. Despite the fact that sensors for diagnostic application should be disposable, the regeneration and reuse of the chip was investigated. It was found that a 3-min immersion in a 50 mM HCl solution could efficiently remove all SARS-CoV-2 antibodies bound onto the RBD-functionalized chip and the chip could be used for more than 30 times (Fig. S5).

### 3.4. Measurement of antibodies in human serum samples

To evaluate the potential of the sensor developed to be applied for the measurement of antibodies against SARS-CoV-2 in real samples, 37 human serum samples, 25 from individuals vaccinated against SARS-CoV-2 and 12 from individuals non-infected and non-vaccinated against SARS-CoV-2 (negative samples), were analyzed. All samples have been also analyzed by an in-house developed ELISA to determine their relative content in antibodies against SARS-CoV-2. In particular, each sample was serially diluted 100, 400, 1600, and 6400-times with assay buffer to receive a titer curve for each one of them and the integrated area under the curve was calculated and divided by 100 to provide a measure of the serum antibody content in arbitrary units. The titer curves for the antibody negative samples are provided in Fig. S6 and for the positive ones in Fig. S7. The values determined by the immersible sensor for all samples in arbitrary units (phase shift multiplied by 10) are depicted in Fig. 5a for the direct binding assay and in Fig. 5b for the assay with the anti-human IgG Fc specific antibody. A cut-off value was determined as the mean +2SD (green line) of the values received for the negative samples. As shown, in case the assay with the direct binding was followed (one step assay), there was 1 out of the 25 samples from vaccinated individuals for which the value determined with the immersible probes was slightly lower than the respective cut-off value. On the other hand, when the assay with the anti-human IgG Fc antibody (two steps assay) was employed, there was an excellent discrimination between the two sample types. In addition, there was a good correlation between the values determined with the immersible probes and those determined by the in-house developed ELISA method (Fig. 5c). In these assays, a secondary anti-IgG antibody (labeled with HRP for ELISA, unlabeled for the sensor) was implemented for signal acquisition, and therefore the anti-SARS-CoV-2 RBD IgGs were determined in both cases. Although the number of samples analyzed is moderate the results obtained support the high reliability of the assay developed for determination of antibodies against SARS-CoV-2 in serum samples.

## 4. Conclusions

An innovative bioanalytical platform based on directly immersible silicon photonic sensors has been demonstrated for the first time. The sensor design alleviates the need for electrical connections, microfluidics and pumps and enables the development of a portable instrument for point-of-need determinations. The analytical potential of the photonic sensor and the accompanying instrumentation were exemplified through the development of a rapid test for the detection of human serum antibodies against the Receptor Binding Domain (RBD) of SARS-CoV-2 Spike 1 protein. The detection could be performed either by directly monitoring the binding of the antibodies contained in the sample or by implementing an additional reaction step with an anti-human IgG Fc specific antibody. In the first case, the assay duration was 10 min and a detection limit of 80 ng/mL in terms of humanized rat antibody against SARS-CoV-2 RBD peptide was achieved, while in the second case, when a secondary antibody was employed, the total assay duration was approximately 20 min and the detection limit 20 ng/mL. Analysis of human serum samples from non-infected non-vaccinated and vaccinated individuals, showed that the proposed platform could completely discriminate vaccinated from non-vaccinated/non-infected individuals, especially when the assay format employing secondary anti-human IgG Fc specific antibody was used. The values obtained for the serum samples tested were well correlated with the antibody titers determined by ELISA for the same samples indicating the potential of the proposed sensor for monitoring the levels of antibodies against SARS-CoV-2 over time in vaccinated or infected individuals. Since the sensors can be functionalized with different recognition molecules, the bioanalytical platform developed can find wide application to the detection of other analytes such as toxins, bacteria, biomarkers, etc. The low energy consumption that allows powering of the measuring

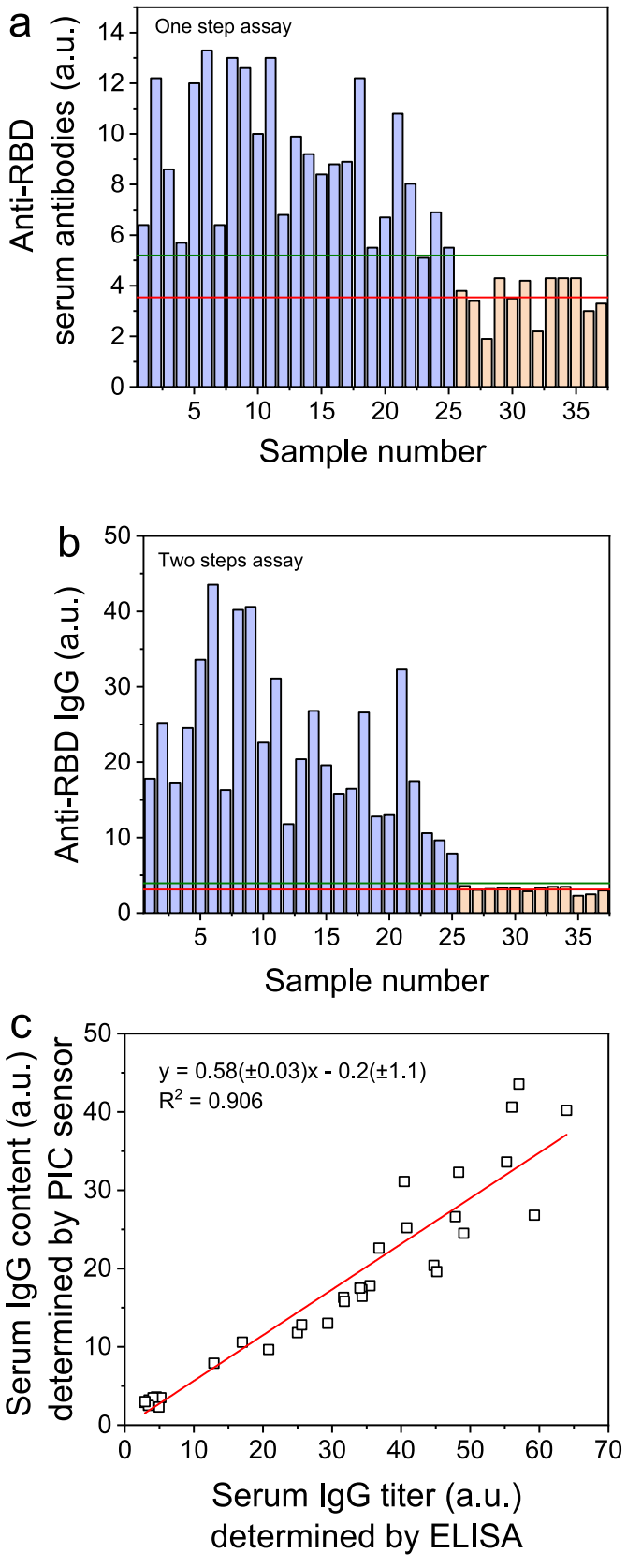


*(caption on next column)*

**Fig. 5.** (a) Anti-RBD antibody values in arbitrary units (a.u.) determined in 37 human serum samples (25 samples from vaccinated donors-blue bars; 12 samples from non-infected non-vaccinated donors-orange bars) with the immersible sensor by monitoring the direct binding of serum antibodies onto the chip antigen. The red line corresponds to the mean and the green one to the mean+2SD of the values obtained from the 12 non-infected non-vaccinated (negative) samples. (b) Anti-RBD IgG values in arbitrary units (a.u.) determined in 37 human serum samples (25 samples from vaccinated donors-blue bars; 12 samples from negative donors-orange bars) with the immersible sensor employing a 10-min immersion in the sample and 5-min immersion in secondary antibody solution. The red and green lines are as in (a). (c) Correlation of values determined in 37 serum samples with the in-house developed ELISA and the immersible PIC sensor. To facilitate comparison between the two methods, the phase shift values determined with the sensor for each sample were multiplied by 10, while the integrated area under the titer curve determined by ELISA was divided by 100.

apparatus through a USB connection to the laptop, its small footprint, and low weight makes the proposed sensing platform ideal for point-of-care/point of need applications. To this direction several issues should be considered such as the ease of use by non-experts and the consumables cost. Currently, the optomechanical adapter that connects and aligns the chip to the bifurcated fiber is fixed onto the fiber and the chip is inserted manually by the user. For point-of-care/point-of-need applications, a new adapter will be designed consisting of two parts, one fixed onto the fiber and the other on the chip, and the two parts will be fasten together in a user friendly manner. Regarding the chip cost, taking into account the current chip dimensions and its fabrication process, for small-scale production (in our research facility) the cost of the chip is approximately 15 euros; however this cost is expected to reach 1.5 euros for mass-scale production (50,000 chips), a very competitive value considering point-of-need applications which require quantitative results. Especially, for non-diagnostic applications, such as in environmental or food analysis which are underway, the cost could be considerably downsized through regeneration and reuse for several times (at least 30 times for the current application) of a single bio-functionalized chip, a quite important feature for low-resources environments.

## CRediT authorship contribution statement

**Michailia Angelopoulou:** Data curation, Formal analysis, Investigation, Methodology, Visualization, Writing – original draft. **Eleni Makarona:** Conceptualization, Methodology, Project administration, Resources, Writing – original draft, Writing – review & editing. **Alexandros Salapatas:** Software, Writing – review & editing. **Konstantinos Misiakos:** Conceptualization, Investigation, Methodology, Resources, Software, Writing – review & editing. **Evgenia Synolaki:** Resources, Validation, Writing – review & editing. **Anastasios Ioannidis:** Resources, Validation, Writing – review & editing. **Stylianos Chatzipanagiotou:** Resources, Writing – review & editing. **Mikael A. Ritvos:** Resources. **Arja Pasternack:** Resources. **Olli Ritvos:** Resources, Writing – review & editing. **Panagiota S. Petrou:** Conceptualization, Investigation, Methodology, Visualization, Resources, Writing – review & editing. **Sotirios E. Kakabakos:** Conceptualization, Methodology, Project administration, Resources, Supervision, Visualization, Writing – review & editing.

## Declaration of competing interest

The authors declare that they have no known competing financial interests or personal relationships that could have appeared to influence the work reported in this paper.

## Data availability

Data will be made available on request.

## Acknowledgments

The authors would like to thank the technical staff of the Nanotechnology and Microsystems Laboratory (Institute of Nanoscience and Nanotechnology, NCSR "Demokritos"), Mr. Athanasios Botsialas of CFN Techniques (Aghia Paraskevi, Greece) for his assistance in the LED PCB board and heat sink fabrication, and Dr. Paschalis Sideras of the Center for Clinical, Experimental Surgery and Translational Research, Biomedical Research Foundation Academy of Athens for helpful discussions about the method validation. The project was partially funded by Athroa Innovations under a Joint Development License Agreement with NCSR "Demokritos".

## Appendix A. Supplementary data

Supplementary data to this article can be found online at https://doi.org/10.1016/j.bios.2022.114570.

## References

Ali, A., Hu, C., Jahan, S., Yuan, B., Saleh, M.S., Ju, E., Gao, S.-J., Panat, R., 2020. Sensing of COVID-19 antibodies in seconds via aerosol jet nanoprinted reduced-graphene-oxide-coated 3D electrodes. Adv. Mater., 2006647, 2020.

Amanat, F., Stadlbauer, D., Strohmeier, S., Nguyen, T.H.O., Chromikova, V., McMahon, M., Jiang, K., Arunkumar, G.A., Jurczyszak, D., Polanco, J., Bermudez-Gonzalez, M., Kleiner, G., Aydillo, T., Miorin, L., Fierer, D.S., Lugo, L.A., Kojic, E.M., Stoever, J., Liu, S.T.H., Cunningham-Rundles, C., Felgner, P.L., Moran, T., García-Sastre, A., Caplivski, D., Cheng, A.C., Kedzierska, K., Vapalahti, O., Hepojoki, J.M., Simon, V., Krammer, F., 2020. A serological assay to detect SARS-CoV-2 seroconversion in humans. Nat. Med. 26 (7), 1033–1036.

Angelopoulou, M., Botsialas, A., Salapatas, A., Petrou, P.S., Haasnoot, W., Makarona, E., Jobst, G., Goustouridis, D., Siafaka-Kapadai, A., Raptis, I., Misiakos, K., Kakabakos, S.E., 2015. Assessment of goat milk adulteration with a label-free monolithically integrated optoelectronic biosensor. Anal. Bioanal. Chem. 407 (14), 3995–4004.

Angelopoulou, M., Petrou, P.S., Makarona, E., Haasnoot, W., Moser, I., Jobst, G., Goustouridis, D., Lees, M., Kalatzi, K., Raptis, I., Misiakos, K., Kakabakos, S.E., 2018. Ultrafast multiplexed-allergen detection through advanced fluidic design and monolithic interferometric silicon chips. Anal. Chem. 90 (15), 9559–9567, 2018.

Antiochia, R., 2021. Developments in biosensors for CoV detection and future trends. Biosens. Bioelectron. 173, 112777.

Banuls, M.-J., González-Pedro, V., Barrios, C.A., Puchades, R., Maquieira, A., 2010. Selective chemical modification of silicon nitride/silicon oxide nanostructures to develop label-free biosensors. Biosens. Bioelectron. 2, 1460–1466.

Cady, N.C., Tokranova, N., Minor, A., Nikvand, N., Strle, K., Lee, W.T., Page, W., Guinon, E., Pilar, A., Gibson, G.N., 2021. Multiplexed detection and quantification of human antibody response to COVID-19 infection using a plasmon enhanced biosensor platform. Biosens. Bioelectron. 171, 112679.

Dzimianski, J.V., Lorig-Roach, N., O'Rourke, S.M., Alexander, D.L., Kimmey, J.M., DuBois, R.M., 2020. Rapid and sensitive detection of SARS-CoV-2 antibodies by biolayer interferometry. Sci. Rep. 10, 21738.

Eckerle, I., Meyer, B., 2020. SARS-CoV-2 seroprevalence in COVID-19 hotspots. Lancet 396 (10250), 514–515.

Feng, M., Chen, J., Xun, J., Dai, R., Zhao, W., Lu, H., Xu, J., Chen, L., Sui, G., Cheng, X., 2020. Development of a sensitive immunochromatographic method using lanthanide fluorescent microsphere for rapid serodiagnosis of COVID-19. ACS Sens. 5, 2331–2337.

Fotis, C., Meimetis, N., Tsolakos, N., Politou, M., Akinosoglou, K., Pliaka, V., Minia, A., Terpos, E., Trougakos, I.P., Mentis, A., Marangos, M., Panayiotakopoulos, G., Dimopoulos, M.A., Gogos, C., Spyridonidis, A., Leonidas, G., Alexopoulos, L.G., 2021. Accurate SARS-CoV-2 seroprevalence surveys require robust multi-antigen assays. Sci. Rep. 11, 6614.

Funari, R., Chu, K.-Y., Shen, A.Q., 2020. Detection of antibodies against SARS-CoV-2 spike protein by gold nanospikes in an opto-microfluidic chip. Biosens. Bioelectron. 169, 112578.

Gajos, K., Angelopoulou, M., Petrou, P., Awsiuk, K., Kakabakos, S., Haasnoot, W., Bernasik, A., Rysz, J., Marzec, M.M., Misiakos, K., Raptis, I., Andrzej Budkowski, A., 2016. Imaging and chemical surface analysis of biomolecular functionalization of monolithically integrated on silicon Mach-Zehnder interferometric immunosensors. Appl. Surf. Sci. 385, 529–542.

Jalkanen, P., Pasternack, A., Maljanen, S., Melén, K., Kolehmainen, P., Huttunen, M., Lundberg, R., Tripathi, L., Khan, H., Ritvos, M.A., Naves, R., Haveri, A., Österlund, P., Kuivanen, S., Jääskeläinen, A., Kurkela, S., Lappalainen, M., Rantasärkkä, K., Vuorinen, T., Hytönen, J., Waris, M., Tauriainen, S., Ritvos, O., Kakkola, L., Julkunen, I., 2021a. A combination of N and S antigens with IgA and IgG measurement is required for accurate SARS-CoV-2 serodiagnosis. J. Infect. Dis. 224, 218–228.

Jalkanen, P., Kolehmainen, P., Häkkinen, H., Pakkanen, S., Huttunen, M., Lundberg, R., Maljanen, S., Reinholm, A., Tauriainen, S., Pasternack, A., Naves, R., Ritvos, O., Österlund, P., Tähtinen, P.A., Ivaska, L., Kuivanen, S., Smura, T., Hepojoki, J., Vapalahti, O., Lempainen, J., Kakkola, L., Kantele, A., Julkunen, I., 2021b. COVID-19 mRNA vaccine induced antibody responses and neutralizing antibodies against three SARS-CoV-2 variants. Nat. Commun. 12, 3991.

Lisboa Bastos, M., Tavaziva, G., Abidi, S.K., Campbell, J.R., Haraoui, L.-P., Johnston, J. C., Lan, Z., Law, S., MacLean, E., Trajman, A., Menzies, D., Benedetti, A., Khan, F.A., 2020. Diagnostic accuracy of serological tests for covid-19: systematic review and meta-analysis. BMJ 370, m2516.

Liu, C., Mao, B., Martinez, V., Chen, X., Li, Y., He, L., Chen, S., Guo, X., Shen, X., Bao, X., Shen, H., Lenna, S., Qian, P., Wu, L., Li, C., 2020. A facile assay for rapid detection of COVID-19 antibodies. RSC Adv. 10, 28041.

Liu, Y., Tan, Y., Fu, Q., Lin, M., He, J., He, S., Yang, M., Chen, S., Zhou, J., 2021. Reciprocating-flowing on-a-chip enables ultra-fast immunobinding for multiplexed rapid ELISA detection of SARS-CoV-2 antibody. Biosens. Bioelectron. 176, 112920.

Luan, E., Shoman, H., Ratner, D.M., Cheung, K.C., Chrostowski, L., 2018. Silicon photonic biosensors using label-free detection. Sensors 18 (10), 1–38.

Makarona, E., Petrou, P., Kakabakos, S., Misiakos, K., Raptis, I., 2016. Point-of-need bioanalytics based on planar optical interferometry. Biotechnol. Adv. 34 (3), 209–233.

Mattioli, I.A., Hassan, A., Oliveira, O.L., Crespilho, F.N., 2020. On the challenges for the diagnosis of SARS-CoV-2 based on a review of current methodologies. ACS Sens. 5, 3655–3677.

Misiakos, K., Raptis, I., Salapatas, A., Makarona, E., Botsialas, A., Hoekman, M., Stoffer, R., Jobst, G., 2014a. Broad-band Mach-Zehnder interferometers as high performance refractive index sensors: theory and monolithic implementation. Opt Express 22 (8), 8856–8870.

Misiakos, K., Raptis, I., Makarona, E., Botsialas, A., Salapatas, A., Oikonomou, P., Psarouli, A., Petrou, P.S., Kakabakos, S.E., Tukkiniemi, K., Sopanen, M., Jobst, G., 2014b. All-silicon monolithic Mach-Zehnder interferometer as a refractive index and bio-chemical sensor. Opt Express 22 (22), 26803–26813.

Misiakos, K., Makarona, E., Hoekman, M., Fyrogenis, R., Tukkiniemi, K., Jobst, G., Petrou, P.S., Kakabakos, S.E., Salapatas, A., Goustouridis, D., Harjanne, M., Heimala, P., Raptis, I., 2019. All-silicon spectrally resolved interferometric circuit for multiplexed diagnostics: a monolithic Lab-on-a-Chip integrating all active and passive components. ACS Photonics 6 (7), 1694–1705.

Okba, N., Muller, M., Li, W., Wang, C., Kessel, C.G., Corman, V., Lamers, M., Sikkema, R., de Bruin, E., Chandler, F., Yazdanpanah, Y., Le Hingrat, Q., Descamps, D., Houhou-Fidouh, N., Reusken, C., Bosch, B.-J., Drosten, C., Koopmans, M., Haagmans, B., 2020. Severe acute respiratory syndrome Coronavirus 2-specific antibody responses in Coronavirus disease patients. Emerg. Infect. Dis. 26 (7), 14780, 1488.

Pagkali, V., Petrou, P.S., Salapatas, A., Makarona, E., Peters, J., Haasnoot, W., Jobst, G., Economou, A., Misiakos, K., Raptis, I., Kakabakos, S.E., 2017. Detection of ochratoxin A in beer samples with a label-free monolithically integrated optoelectronic biosensor. J. Hazard Mater. 323, 75–83, 2017.

Pagkali, V., Petrou, P.S., Makarona, E., Peters, J., Haasnoot, W., Jobst, G., Moser, I., Gajos, K., Budkowski, A., Economou, A., Misiakos, K., Raptis, I., Kakabakos, S.E., 2018. Simultaneous Determination of aflatoxin B1, fumonisin B1and deoxynivalenol in beer samples with a label-free monolithically integrated optoelectronic biosensor. J. Hazard Mater. 359, 445–453.

Psarouli, A., Botsialas, A., Salapatas, A., Stefanitsis, G., Nikita, D., Jobst, G., Chaniotakis, N., Goustouridis, D., Makarona, E., Petrou, P.S., Raptis, I., Misiakos, K., Kakabakos, S.E., 2017. Fast label-free detection of C-reactive protein using broad-band Mach-Zehnder Interferometers integrated on silicon chips. Talanta 165, 458–465.

Rashed, M.Z., Kopechek, J.A., Priddy, M.C., Hamorsky, K.T., Palmer, K.E., Mittal, N., Valdez, J., Flynn, J., Williams, S.J., 2021. Rapid detection of SARS-CoV-2 antibodies using electrochemical impedance-based detector. Biosens. Bioelectron. 171, 112709.

Roda, A., Cavalera, S., Di Nardo, F., Calabria, D., Rosati, S., Simoni, P., Colitti, B., Baggiani, C., Roda, M., Anfossi, L., 2021. Dual lateral flow optical/chemiluminescence immunosensors for the rapid detection of salivary and serum IgA in patients with COVID-19 disease. Biosens. Bioelectron. 172, 112765.

Shakoor, A., Grant, J., Grande, M., Cumming, D.R.S., 2019. Towards portable nanophotonic sensors. Sensors 19 (7), 57–59.

Shaw, A.M., Hyde, C., Merrick, B., James-Pemberton, P., Squires, B.K., Rouslan, V., Olkhov, R.V., Batra, R., Patel, A., Bisnauthsing, K., Nebbia, G., MacMahon, E., Douthwaite, S., Malim, M., Neil, S., Nunez, R.M., Doores, K., Mark, T.K.I., Signell, A. W., Betancor, G., Wilson, H.D., Galão, R.P., Pickering, S., Edgeworthd, J.D., 2020. Real-world evaluation of a novel technology for quantitative simultaneous antibody detection against multiple SARS-CoV-2 antigens in a cohort of patients presenting with COVID-19 syndrome. Analyst 145, 5638.

Steiner, D.J., Cognetti, J.S., Luta, E.P., Klose, A.M., Bucukovski, J., Bryan, M.R., Schmuke, J.J., Nguyen-Contant, P., Sangster, M.Y., Topham, D.J., Miller, B.L., 2020. Array-based analysis of SARS-CoV-2, other coronaviruses, and influenza antibodies in convalescent COVID-19 patients. Biosens. Bioelectron. 169, 112643.

Torrente-Rodrıguez, R.M., Lukas, H., Tu, J., Min, J., Yang, Y., Xu, C., Rossiter, H.B., Wei Gao, W., 2020. SARS-CoV-2 RapidPlex: a graphene-based multiplexed telemedicine platform for rapid and low-cost COVID-19 diagnosis and monitoring. Matter 3, 1981–1998.

Wang, Z., Zheng, Z., Hu, H., Zhou, Q., Liu, W., Li, X., Liu, Z., Wang, Y., Ma, Y., 2020. A point-of-care selenium nanoparticle-based test for the combined detection of anti-SARS-CoV-2 IgM and IgG in human serum and blood. Lab Chip 20, 4255–4261.
Wen, T., Huang, C., Shi, F.-J., Zeng, X.-Y., Lu, T., Ding, S.-N., Yong-Jun Jiao, Y.-J., 2020. Development of a lateral flow immunoassay strip for rapid detection of IgG antibody against SARS-CoV-2 virus. Analyst 145, 5345.
Yakoh, A., Pimpitak, U., Rengpipat, S., Hirankarn, N., Chailapakul, O., Sudkate Chaiyo, S., 2021. Paper-based electrochemical biosensor for diagnosing COVID-19: detection of SARS-CoV-2 antibodies and antigen. Biosens. Bioelectron. 176, 112912.